Available online at www.sciencedirect.com
SCIENCE DIRECT
Physics of the Earth and Planetary Interiors 155 (2006) 219–235
PHYSICS OF THE EARTH AND PLANETARY INTERIORS
www.elsevier.com/locate/pepi

Focal depth distribution using sP depth phase and implications for plate coupling in the Hyuganada region, Japan

Michitaka Tahara [a,*], Hiroshi Shimizu [b], Masao Nakada [c], Yoshihiro Ito [d]

[a] *Department of Earth and Planetary Sciences, Graduate School of Sciences, Kyushu University, Fukuoka 812-8581, Japan*
[b] *Institute of Seismology and Volcanology, Faculty of Sciences, Kyushu University, Shimabara 855-0843, Japan*
[c] *Department of Earth and Planetary Sciences, Faculty of Sciences, Kyushu University, Fukuoka 812-8581, Japan*
[d] *National Research Institute for Earth Science and Disaster Prevention, Tsukuba 305-0006, Japan*

Received 8 July 2005; received in revised form 17 December 2005; accepted 19 December 2005

Abstract

The recurrence interval and magnitude of great interplate earthquakes and characteristics of crustal uplift in the Late Pleistocene indicate clear lateral variations of the plate interaction on the convergent boundary along the Nankai Trough, i.e. relatively less cohesive for the Hyuganada region than for off the Shikoku and Kii Peninsula. The Hyuganada region is characterized by both significant aseismic crustal uplift in the Late Pleistocene and negative free-air gravity anomalies with the maximum magnitude of ∼−130 mgal. In order to examine the relationship for these observations, we investigated the focal depth distribution in the Hyuganada region by using sP depth phases. The focal depth distribution obtained by sP depth phases indicates different seismicity patterns in the southern and northern regions of the forearc. That is, most events for the southern and northern areas are thrust type and normal fault type, respectively. In the central part of the Hyuganada region located in the central area of negative gravity anomalies, however, each type event occurs in clusters and there is a seismicity gap between each cluster. The hypocenters for thrust type events generally coincide with the plate boundary as usual cases. However, most normal fault type events, with hypocenters in the landward side for the thrust type events and *T*-axes parallel to the plate boundary, occur in the crust or around the plate boundary of the forearc and the epicenters coincide with the peak position of negative gravity anomalies. The correlation between the seismicity and gravity anomaly suggests that the buoyancy inferred from negative gravity anomalies may cause the observed tensile events and a few relatively small asperities of the observed M_w 7 class earthquakes on the convergent boundary. This may be related to relatively less cohesive coupling around the Hyuganada region compared with that for off the Shikoku.

Keywords: Depth phase; Plate coupling; Focal mechanism; Gravity anomaly; Philippine Sea Plate

1. Introduction

The Philippine Sea Plate (PHS) is subducting northwestward (∼5 cm yr^{-1}) beneath the Southwest (SW) Japan Arc along the Nankai Trough (e.g. Ando, 1975; Seno et al., 1993). Along this island arc (Fig. 1), however, several distinctive geological and geophysical phenomena have been observed as reviewed by Nakada et al. (2002). Cape Muroto and Ashizuri in Shikoku and Kii Peninsula have been uplifted by interplate earthquakes with a recurrence interval of 100–200 years (Ando, 1975; Kumagai, 1996), and the uplift reaches ∼150 m during the past 120 thousand years (kyr) (Ota and Omura, 1991).

* Corresponding author. Tel.: +81 92 642 2647; fax: +81 92 642 2684.
E-mail address: tahara@geo.kyushu-u.ac.jp (M. Tahara).

0031-9201/$ – see front matter © 2006 Elsevier B.V. All rights reserved.
doi:10.1016/j.pepi.2005.12.004

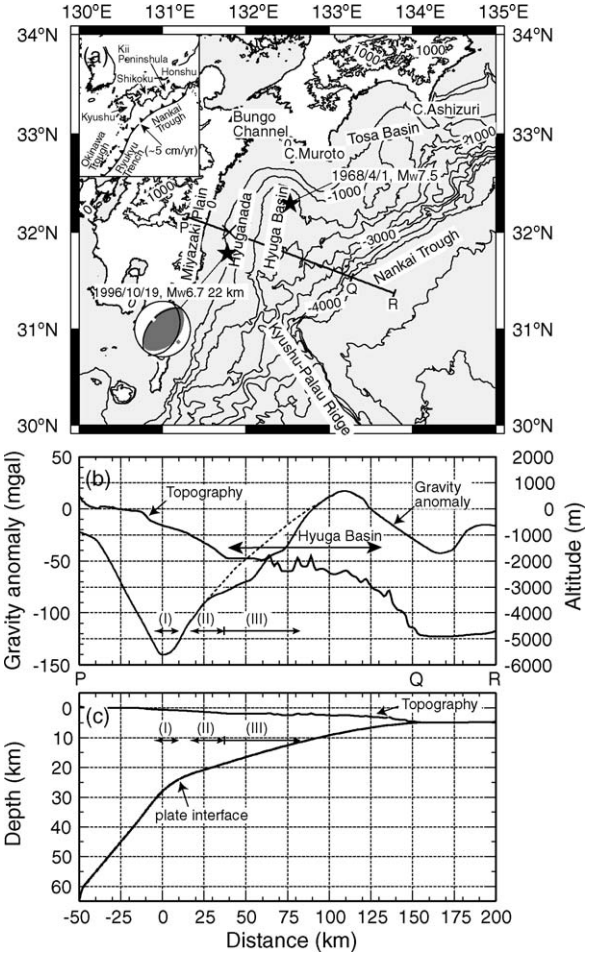

Fig. 1. (a) Location map used in this study. The cross (×) indicates the peak position of negative free-air gravity anomaly (see Fig. 2b). Focal mechanism for an event on October 19, 1996, referred to as HG1996 here, and the epicenter for an event on April 1, 1968 are shown. (b) Topography and observed gravity anomalies by Kono and Furuse (1989) (Bouguer gravity anomaly for land region and free-air gravity anomaly for ocean region) along the line P–R. The point of 0 km (× in subpart (a)) corresponds to the peak position of the negative gravity anomaly for region B in Fig. 2b. The horizontal axis for subparts (b) and (c) and Figs. 6–10 represents the distance (km) from the dashed line in Fig. 2c. Region I corresponds to the zone where most events are tensile (western part), and region II corresponds to the zone where most events are thrust types (eastern part) in Fig. 10. The dashed part of the gravity anomaly in subpart (b) is a hypothetical regional anomaly discussed in the text. (c) The vertical view of the plate boundary and topography along the line P–R. Regions I and II correspond to those for subpart (b).

On the other hand, the Miyazaki Plain has been uplifting aseismically, and the uplift amounts to 10–120 m during the past ∼120 kyr (Nagaoka, 1986; Nagaoka et al., 1991; see also Nakada et al., 2002).

The seismicity patterns of thrust type earthquakes on the plate boundary for these regions are significantly different in both the magnitude (M) and recurrence interval. In the Hyuganada region between the Miyazaki Plain and Hyuga Basin, earthquakes with $6.5 < M < 7.5$ usually occur at 10–20 years interval and the maximum magnitude is at most 7.5 (Utsu, 1974). On the other hand, the maximum magnitude for off the Shikoku is greater than 8 and its recurrence interval is 100–200 years (Ando, 1975; Kumagai, 1996). In the Hyuganada region, there are a few relatively small asperities of the M_w 7 class earthquakes, whereas there is a major asperity of the M_w 8 class earthquakes for off the Shikoku (e.g. Kawasaki, 2004). That is, stresses accumulated through the process related to PHS subduction are partly released by slip of small asperities at frequent intervals in the Hyuganada region. In a period of 100–200 years, however, the total stress release in the Hyuganada region may be similar to that for off the Shikoku if we consider the magnitude and recurrence intervals for both regions. The observed characteristics for off the Miyazaki Plain may be supported from the crustal strains deduced from GPS data (Kato et al., 1998). In addition, co-seismic slip and post-seismic slip occur in the deep portion of cohesive region around the Hyuganada (Yagi et al., 2001) whereas slow slip events are observed around Bungo Channel (Hirose et al., 1999). Also, deep long-period tremors are observed distinctively in a non-volcanic region for SW Japan (Obara, 2002).

Hyndman et al. (1995) suggested that the strength of interplate coupling depends on temperature around plate boundary, and lower limits of coupling zone correspond to the isotherm of 350 °C. For SW Japan, upper plate events occur above about 20 km depth (Nakamura et al., 1997), indicating that the coupled zone along the Nankai Trough is about 20 km depth. The downdip limit of rupture area of 1946 great interplate earthquake is at a horizontal distance of 140 km from trench axis (Ando, 1975). Wang and Suyehiro (1999) explained the difference of plate coupling between Northeast (NE) Japan and SW Japan based on the plate coupling using the static friction law. In the Hyuganada region, the coupled zone is about 15–25 km depth as shown later (Fig. 10) and the horizontal distance from trench axis is about 150 km (Fig. 1c), consistent with the situation of the Nankai Trough for off the Shikoku. That is, the plate coupling proposed by Wang and Suyehiro (1999) would not explain the different seismicity patterns for both regions.

The Miyazaki Plain and the western part of the Hyuga Basin are also characterized by significant negative gravity anomalies with the maximum magnitude of ∼−130 mgal as shown in Figs. 2b and 1b (Kono and Furuse, 1989; Geological Survey of Japan, 2000). Nagaoka et al. (1991) suggested that the low-density

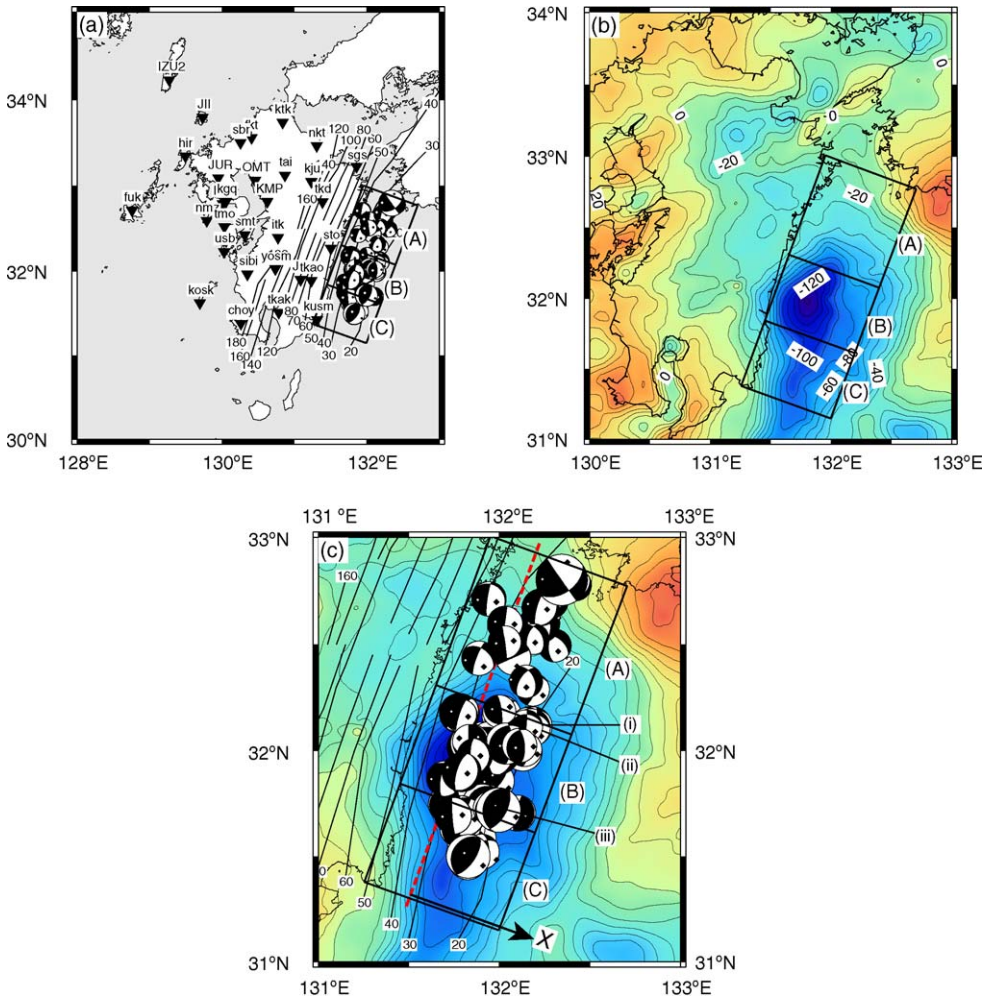

Fig. 2. (a) The distribution of earthquakes by SEVO and focal mechanisms by NIED. Inverted triangles show seismic stations used here. Contour lines show the surface of the subducting slab determined by hypocenter distribution of micro-earthquakes occurred in and around Kyushu (Uehira et al., 2001). (b) Observed gravity anomalies (mgal) digitized from the map by Kono and Furuse (1989) (Bouguer gravity anomalies with a terrain correction density of 2670 kg m^{-3} for land region and free-air gravity anomalies for ocean region). (c) The distribution of earthquakes by SEVO and focal mechanisms by NIED. In this study, we investigate the focal depths for regions A–C separately. The bold dashed line corresponds to the origin (distance = 0) for Figs. 1b, c and 6–10, and that for region B is located on the peak position of negative free-air gravity anomalies. (i)–(iii) denote earthquakes whose waveforms are shown in Fig. 4.

material associated with low gravity anomalies is caused by a subduction of the Kyushu Palau ridge, remnant arc related to the back-arc spreading of the Sikoku Basin (Kobayashi and Nakada, 1978). This problem is, however, still controversial (Kamata and Kodama, 1993; Nakada et al., 2002), and there is no quantitative answer for this.

In the Hyuganada Region, it is noted that the coupled zone of ∼25 km depth is consistent with the position of minimum gravity anomaly (Fig. 1b and c). Wells et al. (2003) investigated published areas of high coseismic slip, or asperities, for 29 of the largest Circum-Pacific megathrust earthquakes, and indicated the relationships between basin-centered asperity, gravity low, subsidence, subduction erosion and seismogenesis. Coseismic slip on the plate boundary thrust is usually nonuniform and contains regions of higher slip or seismic moment release commonly known as asperities (e.g. Lay and Kanamori, 1981). Wells et al. (2003) indicated that the asperity areas occur beneath the deep-sea terraces and forearc basins generally coinciding with prominent low free-air gravity anomaly. Their works confirmed Mogi's (1969) suggestion that great earthquake slip coincides with offshore topographic depressions. Although Wells

et al. (2003) indicated the relationship using the asperity area of 1968 Hyuganada earthquake (Yagi and Kikuchi, 2003), the area for asperity is away from that for significant negative gravity anomalies as discussed later in detail.

On the other hand, Nakada et al. (2002) quantitatively indicated that the underplating load inferred from the observed negative gravity anomalies can explain the crustal uplift around the Miyazaki Plain. That is, they estimated the mass deficiency below 11 km depth using the observed gravity anomalies and crustal structure above 11 km depth (Tashiro et al., 1999). Then, they evaluated the plate (crust) deformation caused by the underplating load existing underneath the Moho or the upper crust, and indicated that the observed crustal uplift can be reasonably explained by this model. Similar observations, crustal uplift in the forearc region, for the Raukumara Peninsula, New Zealand, have been explained by an accumulation of sediments associated with subduction (Walcott, 1987; Reyners and McGinty, 1999).

The underplating load beneath the forearc will significantly affect the cohesive state between the subducting Philippine Sea Plate and overriding plate, although the underplating load has not been ascertained quantitatively. The steady upward movement ($\sim$1 mm yr^{-1}) of the overriding plate, inferred from the uplift in the Late Pleistocene around the Miyazaki Plain, will weaken the plate coupling. If the underplating load model is true, then horizontal tension of the overriding plate is expected although it depends on the magnitude of the buoyancy. Also, the Hyuganada region is an important place to examine the relationship between the asperities and prominent free-air gravity anomalies indicated by Wells et al. (2003).

Here we analyze the focal mechanisms and focal depths for events in the Hyuganada region in order to examine the relationship between the seismicity pattern and gravity anomalies. This may provide important clues in understanding spatial variations for the occurrence of great earthquakes along the forearc associated with the subducting Philippine Sea Plate. It is, however, difficult to determine these seismic parameters because the Hyuganada region is suboceanic and the observation stations are only located on the land region (see Fig. 2a). To determine the focal depths precisely, we use a converted wave from S- to P-wave, i.e. sP depth phase, dominantly sensitive to the focal depth (Stein and Wiens, 1986; Umino et al., 1995). The difference of arrival times between the direct P-wave and converted S-wave (sP − P time) depends on both the focal depth and seismic-velocity structure.

2. Hypocenter distribution and focal mechanism solutions in the Hyuganada region

In order to examine the relationship between the seismicity and gravity anomaly in the Hyuganada region, it is necessary to determine the focal depth and focal mechanism precisely. Fig. 2a and c show the distribution of earthquakes with focal mechanism solutions analyzed in this study (64 events). The hypocenters for events in Fig. 2 were determined by Institute of Seismology and Volcanology, Kyushu University (SEVO), using P- and S-wave arrivals at the seismic stations of Kyushu University, Kagoshima University, Japan Meteorological Agency (JMA) and National Research Institute for Earth Science and Disaster Prevention (NIED). In this study, we adopt these hypocenters as initial values for the hypocenter re-determination using sP − P times. The depth (km) of the surface of subducting Philippine Sea Plate is also depicted in this figure (Uehira et al., 2001). The focal mechanism solutions in Fig. 2 were determined by NIED using the moment tensor (MT) analysis (Fukuyama et al., 1998). NIED adopts moment tensor inversion method, and the moment tensor solutions and centroid depths are automatically determined from waveform data obtained by real-time seismographic network and JMA's initial seismic information data (Fukuyama et al., 1998). The centroid depth by NIED has been determined by putting a point source every 3 km interval from 5 km depth, and has been published (http://www.fnet.bosai.go.jp/freesia/event/dreg.html). In this method, the centroid depths are only determined, whereas the centroid locations are determined by Harvard centroid moment tensor inversion method (Dziewonski et al., 1981).

In order to examine the focal mechanisms, we determined focal solutions by using P-wave first motions for 24 events with $M_w \geq 3.5$ from January 1997 to September 2001, for which MT solutions by NIED are also available. Focal mechanism solutions based on first motion polarity data and MT solutions are shown in Fig. 3. Although the focal solutions based on first motion polarity data are almost similar to the MT solutions, the solutions for some events are discrepant. These first motion polarities are limited in azimuth because the events examined here occur beneath the ocean floor and there are no observation stations around epicenters. That is, the focal mechanisms based on first motion polarity are less reliable compared with those by MT solutions. In addition, the first motion solution reflects the process of rupture initiation whereas MT solution represents an average source process (Scott and Kanamori, 1985).

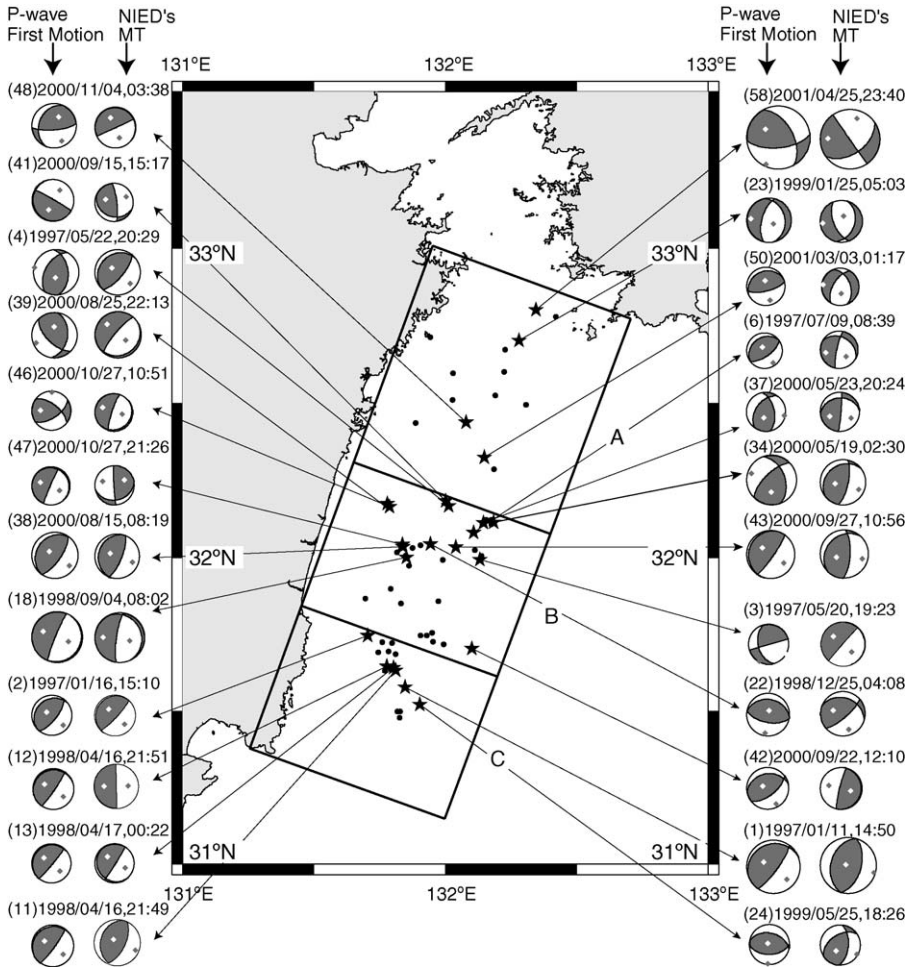

Fig. 3. Focal mechanisms (lower hemisphere projection) based on first motion polarity data solutions (left side) and MT solutions (right side).

That is, MT solutions represent more regional stress field although first motion polarities are vulnerable to the influence of local stress field and inhomogeneous structure. Furthermore, the number of data determined by first motion polarities is limited. In this study, we therefore adopt MT solutions by NIED. Fig. 2c shows the focal mechanisms for 64 events with $M_w \geq 3.5$ determined by MT solutions. In the Hyuganada region, normal fault type earthquakes occupy more than 40% in the events shown in Fig. 2c. This tendency seems to be unique compared with other subduction zones such as Tohoku region, characterized by thrust type earthquakes around the forearc (Kanamori, 1977).

3. sP depth phase

As discussed above, normal fault type earthquakes frequently occur in the Hyuganada region. It is, however, difficult to determine the focal depths for these events as seen from the results by three organizations (Table 1). For example, the focal depths for event 1 in Table 1 are 15.3 km for SEVO, 40.32 km for JMA and 26 km for NIED. Then, we use depth phases to determine the focal depths more accurately than three organizations. Travel time difference between depth phases such as pP and sP phases and P-wave mainly depends on the focal depth (Stein and Wiens, 1986; Umino et al., 1995). In this study, we relocate focal depths using sP depth phase. Kennett and Engdahl (1991) numerically indicated the existence of sP phase for velocity model of iasp91, and Umino et al. (1995) reported that sP phases are observed at epicentral distances for greater than 150 km. The definition of sP phase is as follows (e.g. Umino et al., 1995): an upgoing S-wave that is subsequently reflected and converted to a P-wave at the top of the crust and which finally reaches stations at the surface. The difference of arrival-times between the direct P-wave and the converted S-wave (sP − P time)

Table 1
Hypocenters of SEVO, JMA and NIED and those determined by sP − P times

No.	Date (JST)	SEVO				JMA		NIED		sP2(Fig. 9a)			sP3(Fig. 9b)		
		Lat.	Lon.	Focal depth (km)	M	Focal depth (km)	M_{JMA}	Focal depth (km)	M_w	Lat.	Lon.	Focal depth (km)	Lat.	Lon.	Focal depth (km)
1	1997/01/11, 14:50:21.71	31.5785	131.8462	15.3	5.1	40.32	4.8	26	5.4	31.5722	131.8294	21.08	31.5512	131.8332	28.18
2	1997/01/16, 15:10:36.92	31.7466	131.7048	15.2	3.8	36.14	3.5	23	3.9	31.7519	131.7184	9.34	31.7443	131.6980	17.91
3	1997/05/20, 19:23:50.84	31.9940	132.1308	3.3	3.8	24.00	3.6	8	4.2	31.9832	132.1247	11.77	31.9815	132.1238	13.04
4	1997/05/22, 20:29:30.33	32.1687	132.0126	5.7	4.3	17.51	3.9	29	4.3	32.1693	131.9901	13.85	32.1659	131.9728	21.79
5	1997/05/28, 14:00:49.58	32.0307	131.8751	9.4	3.6	24.71	3.6	32	3.6	32.0306	131.8659	11.01	32.0262	131.8530	19.19
6	1997/07/09, 08:39:13.16	32.0818	132.1077	14.0	3.4	33.23	3.5	35	3.6	32.0816	132.0994	18.09	32.0824	132.0960	20.50
7	1997/10/10, 14:37:40.19	31.7227	131.7981	13.2	3.8	29.19	3.9	32	4.0	31.7157	131.8013	15.43	31.6847	131.8253	23.72
8*	1997/10/21, 16:46:10.67	32.7126	131.9426	28.6	3.9	46.58	3.9	53	3.8	32.7098	131.9502	14.61	32.7111	131.9480	21.24
9	1997/10/24, 09:38:44.43	32.4943	132.3067	13.1	3.7	19.59	3.9	26	3.6	32.4916	132.3131	17.06	32.4901	132.3161	18.73
10	1997/11/06, 14:27:56.75	31.7251	131.7597	25.1	3.8	38.65	3.8	14	3.9	31.7443	131.7534	15.62	31.7229	131.7614	26.05
11	1998/04/16, 21:49:03.77	31.6343	131.8107	19.1	4.0	28.69	3.9	26	4.4	31.6540	131.8214	12.88	31.6413	131.8115	17.22
12	1998/04/16, 21:51:34.41	31.6472	131.7764	19.5	3.9	30.63	3.8	8	4.2	31.6482	131.8157	11.57	31.6480	131.7911	16.44
13	1998/04/17, 00:22:56.59	31.6426	131.8033	17.2	3.7	30.83	3.6	11	3.7	31.6472	131.8236	11.75	31.6438	131.8086	15.81
14	1998/04/19, 21:03:31.24	31.8675	131.6967	26.9	3.9	42.70	3.8	23	3.9	31.8633	131.7470	11.94	31.8669	131.7109	20.78
15	1998/04/22, 06:55:09.84	32.0171	131.8165	22.9	4.1	33.52	4.0	38	4.2	32.0128	131.8420	14.60	32.0172	131.8143	24.05
16	1998/06/28, 08:37:44.93	31.4793	131.8261	14.4	4.1	27.92	3.8	20	4.2	31.4779	131.8187	16.30	31.4767	131.8104	18.30
17	1998/07/23, 20:07:26.79	31.7559	131.9494	11.9	4.3	23.68	4.1	23	4.4	31.7568	131.9391	16.07	31.7568	131.9349	17.93
18	1998/09/04, 08:02:37.90	32.0005	131.8525	21.5	4.8	32.38	4.5	23	4.7	32.0117	131.8656	11.22	32.0034	131.8557	19.15
19	1998/09/15, 08:16:22.19	32.6002	132.2236	17.6	4.5	36.84	4.2	38	4.4	32.6093	132.2251	21.09	32.5970	132.2475	30.50
20	1998/09/27, 08:43:46.04	31.8574	131.9742	11.8	4.2	26.53	4.2	29	4.3	31.8442	131.9652	20.87	31.8325	131.9691	27.12
21*	1998/09/28, 02:50:22.10	32.0397	131.9051	21.8	4.5	37.03	4.4	62	4.5	32.0332	131.9347	12.86	32.0387	131.9111	19.75
22*	1998/12/25, 04:08:32.40	32.0438	131.9440	6.1	4.1	18.08	4.0	65	4.3	32.0455	131.9321	10.75	32.0480	131.9141	17.02
23	1999/01/25, 05:03:12.77	32.7028	132.2808	24.8	4.2	42.38	4.0	35	4.0	32.7032	132.2708	18.81	32.7026	132.2867	27.27
24	1999/05/25, 18:26:10.51	31.5225	131.9025	13.5	3.8	37.89	3.8	26	3.9	31.5208	131.8945	16.69	31.5204	131.8888	18.52
25	1999/06/24, 21:18:40.52	32.0073	131.8507	20.0	3.8	30.18	3.8	29	4.0	32.0040	131.8634	15.84	32.0096	131.8378	25.24
26	1999/10/10, 02:13:30.57	32.2869	132.1852	−7.6	3.6	0.49	3.6	20	3.6	32.2844	132.1931	15.07	32.2838	132.1941	16.85
27	1999/11/10, 08:01:50.34	32.1095	132.1405	−1.2	3.5	15.14	3.5	23	3.5	32.1090	132.1356	16.10	32.1091	132.1338	17.81
28	1999/11/29, 07:16:46.92	32.5964	132.0302	20.1	3.8	33.26	3.8	38	3.9	32.5682	132.0324	15.63	32.5673	132.0280	26.53
29	1999/12/22, 20:17:27.13	31.9921	131.9906	19.8	5.4	38.72	4.8	29	4.9	31.9920	131.9925	19.07	31.9934	131.9781	25.95
30	2000/01/06, 08:43:46.97	31.6323	131.7702	19.5	3.9	29.39	3.8	26	4.0	31.6446	131.7894	10.81	31.6365	131.7819	15.74
31	2000/02/22, 22:49:49.74	31.8506	131.8307	20.4	3.6	29.31	3.7	26	3.7	31.8483	131.8489	11.53	31.8498	131.8365	17.97
32	2000/03/08, 12:15:25.82	32.6724	132.2272	21.7	3.9	38.42	3.8	41	4.1	32.6716	132.2193	13.19	32.6721	132.2254	19.85
33	2000/05/17, 12:04:08.96	32.1217	132.1755	1.4	4.5	21.07	4.1	20	4.1	32.1184	132.1763	15.81	32.1184	132.1757	17.33
34	2000/05/19, 02:29:58.84	32.1147	132.1829	1.6	4.7	22.93	4.4	20	4.3	32.1133	132.1822	16.11	32.1132	132.1812	17.45
35	2000/05/19, 04:07:00.19	32.1222	132.1566	0.0	3.5	17.43	3.5	20	3.8	32.1225	132.1532	15.32	32.1204	132.1559	16.99
36	2000/05/23, 08:56:22.25	32.1078	132.1746	0.4	4.5	20.19	4.4	17	4.2	32.1014	132.1787	14.97	32.1014	132.1797	16.31
37	2000/05/23, 20:24:44.87	32.1134	132.1455	0.8	3.7	18.42	3.7	20	3.7	32.1105	132.1422	16.33	32.1113	132.1399	18.08

38	2000/08/15, 08:18:56.65	32.0354	131.8386	18.0	4.4	22.28	4.2	32	4.3	32.0281	131.8573	13.94	32.0442	131.8155	22.98
39	2000/08/25, 22:12:54.14	32.1759	131.7792	25.8	4.3	37.20	4.1	41	4.4	32.1577	131.8481	12.56	32.1692	131.8017	21.30
40	2000/09/08, 20:40:44.53	32.0057	132.1385	12.2	4.0	25.69	3.8	23	3.8	32.0165	132.1130	17.70	32.0211	132.1037	19.75
41	2000/09/15, 15:17:27.61	32.1847	132.0000	14.7	4.0	27.28	3.8	32	3.6	32.1877	131.9870	18.61	32.1914	131.9658	29.32
42	2000/09/22, 12:10:12.39	31.7048	132.1007	25.0	4.0	42.97	3.9	26	4.0	31.7273	132.0975	13.77	31.7277	132.0978	13.53
43	2000/09/27, 10:56:45.99	32.0337	132.0392	21.6	4.6	15.96	4.2	26	4.6	32.0282	132.0707	16.66	32.0301	132.0565	18.99
44	2000/09/27, 17:43:36.50	32.024	132.1121	16.2	3.6	25.60	3.5	23	3.8	32.0210	132.1235	13.40	32.0233	132.1152	15.48
45	2000/10/23, 12:30:19.11	32.5253	132.1905	18.1	3.5	30.47	3.6	32	3.4	32.5224	132.1949	24.16	32.5087	132.2078	34.95
46	2000/10/27, 10:51:03.21	32.1659	131.7882	25.7	3.7	32.19	3.7	32	3.6	32.1475	131.8412	15.38	32.1681	131.7924	24.19
47*	2000/10/27, 21:26:07.92	32.0427	131.8361	24.9	3.6	38.14	3.6	53	3.8	32.0413	131.8636	15.08	32.0421	131.8367	24.51
48	2000/11/04, 03:38:33.49	32.4392	132.0779	16.7	4.2	30.61	3.9	32	3.9	32.4388	132.0786	20.70	32.4241	132.0863	33.28
49	2001/03/02, 18:52:57.01	32.4352	131.8875	27.7	4.2	37.59	3.8	32	3.8	32.4257	131.9380	12.79	32.4336	131.9062	21.67
50	2001/03/03, 01:17:34.27	32.3248	132.1474	11.1	3.6	24.38	3.5	29	3.6	32.3268	132.1419	18.34	32.3228	132.1435	24.23
51	2001/03/06, 15:43:42.49	31.7473	131.9298	14.3	4.4	26.45	4.1	26	4.4	31.7462	131.9241	16.63	31.7445	131.9199	18.75
52	2001/03/06, 19:36:04.81	31.7466	131.9066	15.5	4.7	27.31	4.3	26	4.5	31.7455	131.9011	17.44	31.7408	131.8950	22.31
53	2001/03/09, 03:43:37.69	31.6945	131.7843	22.1	4.2	37.23	4.0	20	4.4	31.7069	131.8104	11.71	31.7011	131.7942	17.52
54	2001/03/09, 03:46:03.96	31.6864	131.8108	22.4	4.3	35.54	4.0	23	4.2	31.7010	131.8170	16.36	31.6788	131.8081	25.25
55	2001/04/09, 01:18:05.61	31.6919	131.7457	25.9	3.7	38.87	3.7	20	4.1	31.7167	131.7699	14.92	31.6985	131.7459	23.71
56	2001/04/14, 08:51:26.90	31.7272	131.9527	10.7	3.6	27.76	3.5	17	3.9	31.7131	131.9443	18.48	31.7074	131.9470	20.51
57	2001/04/16, 18:58:10.08	32.7779	132.4212	21.6	3.6	35.30	3.7	14	3.5	32.7823	132.3932	12.61	32.7816	132.3991	14.87
58	2001/04/25, 23:40:08.21	32.8019	132.3447	29.5	6.0	41.54	5.6	35	5.7	32.7996	132.3366	20.74	32.8028	132.3433	28.85
59	2001/07/13, 07:13:14.91	31.9741	131.8626	21.9	4.0	34.56	3.9	29	3.9	31.9686	131.8787	17.59	31.9797	131.8505	27.15
60	2001/07/21, 20:24:58.72	32.5104	132.0284	22.8	3.5	31.35	3.5	35	3.6	32.5045	132.0332	17.26	32.5118	132.0239	29.80
61	2001/07/25, 05:10:44.41	31.8985	131.7921	23.6	4.4	32.40	4.1	23	4.3	31.8798	131.8386	16.15	31.9003	131.7880	24.49
62	2001/08/29, 23:27:13.16	31.4988	131.8178	15.6	3.6	26.55	3.7	23	3.7	31.5000	131.8283	13.64	31.4988	131.8172	15.71
63	2001/08/30, 05:52:26.94	31.4994	131.8283	15.4	4.9	28.17	4.6	23	4.8	31.4987	131.8151	17.80	31.4948	131.8029	20.92
64	2001/09/17, 11:21:44.95	31.7185	131.9947	6.4	5.1	28.31	4.7	26	4.9	31.7230	131.9762	14.05	31.7239	131.9707	16.28

Focal mechanisms for events denoted by asterisk are not included in Fig. 10.

depends on both the focal depth and the seismic-velocity structure.

Umino et al. (1995), for example, relocated focal depth in Tohoku district using sP depth phase. As a result, they could show a more detailed double seismic zone in Tohoku district. The characters of sP phase obtained by them are as follows: (i) X phase is mainly observed in the vertical and radial components, (ii) X phase is generally observed at epicentral distances for greater than 150 km, (iii) the apparent velocity of X phase is slower than direct P-wave and faster than direct S-wave, (iv) the period of X phase is slightly longer than direct P-wave and almost the same as direct S-wave and (v) the amplitude of X phase changes for each earthquakes and is about 50–200% of direct P-wave.

We can find later phases with dominant vertical and radial components for 90% events examined here at epicentral distance greater than 200 km, and identified sP phase by above characters. Fig. 4 shows vertical components for three events indicated by (i)–(iii) in Fig. 2c, in which sP phases have been identified. Dotted lines indicate direct P or Pn phases and dashed lines indicate direct S phase. sP phases are indicated by solid lines. The results clearly indicate that the travel time difference, sP − P time, is insensitive to the epicentral distance for greater than 200 km. Fig. 5 shows the three components of seismograms for the event in Fig. 4c at stations Hirado (hir) and Fukue (fuk) in Fig. 2a; vertical (UD), NS, EW, and particle motions of P and sP phases for these observations. It is confirmed that sP phases identified here have dominant vertical and radial components. The large amplitude of these phases discussed above and theoretical travel-times discussed later indicate that the phases identified here are not pP phases.

4. Focal depth determined by sP depth phase

Fig. 6 shows the distributions of arrival-time differences between sP and direct P phases (sP − P time) for regions A–C shown in Fig. 2. The horizontal axis for Figs. 6–10 represents the distance (km) from the dashed line in Fig. 2c, and the origin (distance = 0) in region B corresponds to the peak position of negative free-air gravity anomalies. While some coastward trends associated with the subducting slab may be expected for observed sP − P times, observed sP − P times are, however, relatively uniform. In this section, we determine focal depths using observed sP − P times.

Hokkaido University, Tohoku University and University of Tokyo carried out seismic reflection experiments in the Hyuganada region using air gun and ocean-bottom seismometer in 1995 (Ichikawa, 1997). Ichikawa (1997) analyzed these data and determined a detailed crustal structure for the Hyuganada region, and indicated a remarkable thick sedimentary layer with a thickness of about 5 km. The P-wave velocity structure in the Hyuganada region was constructed by data along about the WNW-ESE traverse crossing the peak position of negative gravity anomaly revealed for region B in Fig. 2b. Here we adopt this model for regions A and C because we have no observations except for model by Ichikawa (1997). Therefore, the focal depths determined by the observed sP − P times for region B are more reliable compared with those for regions A and C. In the Miyazaki Plain, Research Group for Explosion Seismology carried out seismic explosion experiments in 1994 and 1996. Based on these data, Tashiro et al. (1999) determined P-wave velocity structure above 11 km depth using arrival time and ray tracing. Nakamura (2002) estimated the depth of the Moho discontinuity in Kyushu using the converted waves observed for intermediate earthquakes. Uehira et al. (2001) determined a detailed structure of the deep seismic zone in Kyushu district.

In western part of Kyushu, however, detailed crustal structure has not been reported yet. Then, we adopted a following synthesized velocity structure model, i.e. the depth of the Moho determined by Nakamura (2002), the depth of the Conrad discontinuity for Tohoku district (Iwasaki et al., 2001) and the structure by SEVO for the depth above the Conrad discontinuity. The following results are, however, insensitive to an adoption of this synthesized model, because the travel time difference for sP and P, sP − P time, is insensitive to the structure for this region. We adopted 7.8 km s^{-1} for the mantle velocity on the landward side by considering the results of 7.74 km s^{-1} by Fukumitsu et al. (1997), 7.8 km s^{-1} by Ono et al. (1978) and 7.9 km s^{-1} by SEVO. The reported Pn velocity beneath the land area for northeastern Japan Arc is ∼7.5 km s^{-1} and that near the Japan Sea coast is 8.2 km s^{-1} (Yoshii, 1979). The value adopted here is intermediate for these reported values. S-wave velocity beneath a conversion point for sP phase is most effective to focal depth. That is, the S-wave velocity structure, particularly for the thick sedimentary layer discussed above, plays an important role on determining sP − P times for events examined here. However, S-wave velocity structure around the Hyuganada region has not been reported yet. Then, we adopted experimental data of compressional velocity, V_p, and shear velocity, V_s, for unconsolidated sediments and sedimentary, metamorphic and igneous rocks by Ludwig et al. (1970).

Fig. 7a depicts the two-dimensional P-wave velocity structure model adopted here, which is based on sev-

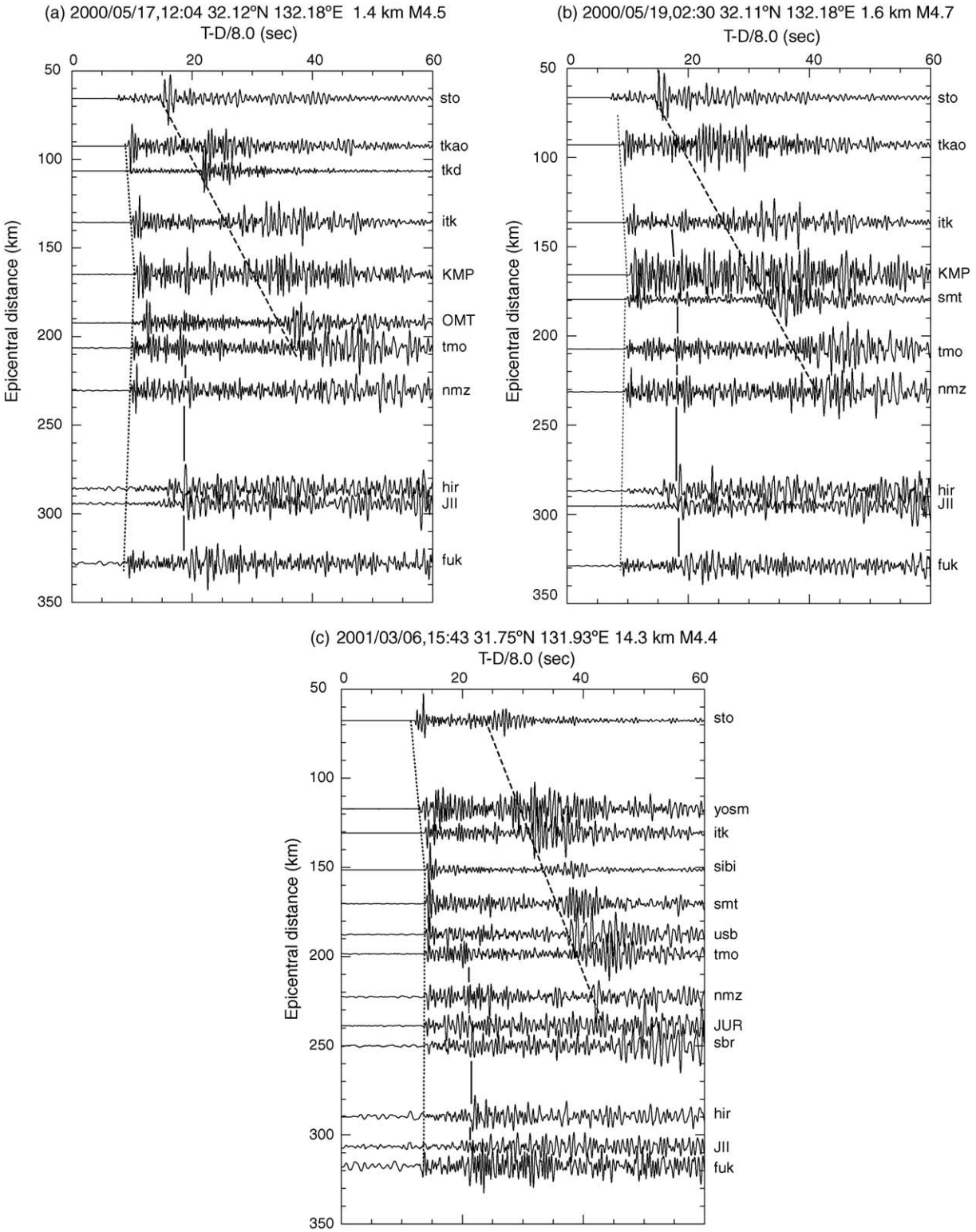

Fig. 4. (a–c) Three examples of seismograms showing distinct later phases between P and S phases. Vertical components reduced by 8.0 km s^{-1} are shown. Dotted, solid and dashed lines indicate P or Pn, sP and S phases, respectively.

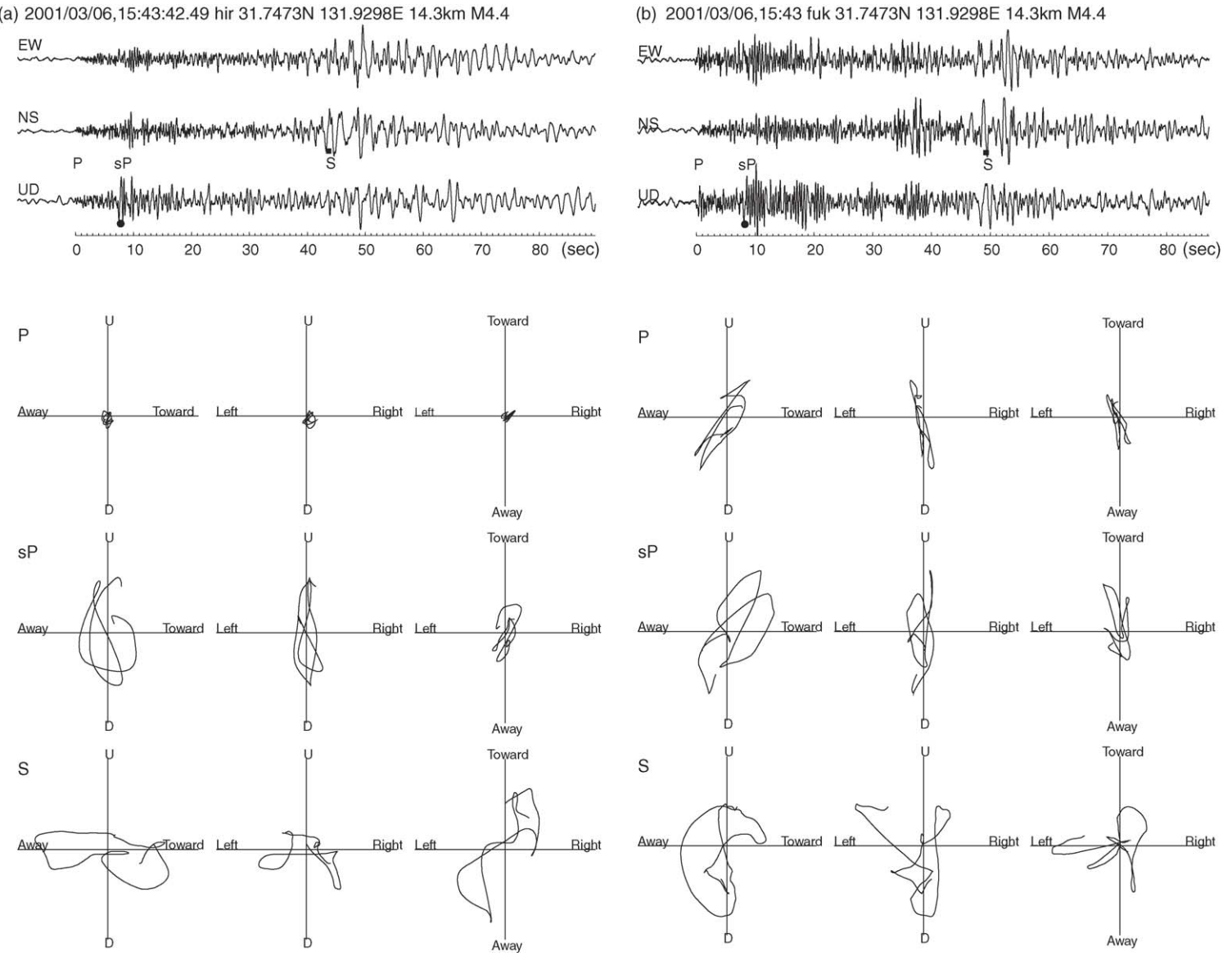

Fig. 5. Three components (UD, NS and EW) of seismograms and particle motions of P, sP and S phases. (a) For Hirado (hir) and (b) for Fukue (fuk) for seismograms for Fig. 4c. Solid circle and solid square indicate sP and S phases, respectively. Particle motions of each phase for 1 s are projected in three mutually orthogonal planes.

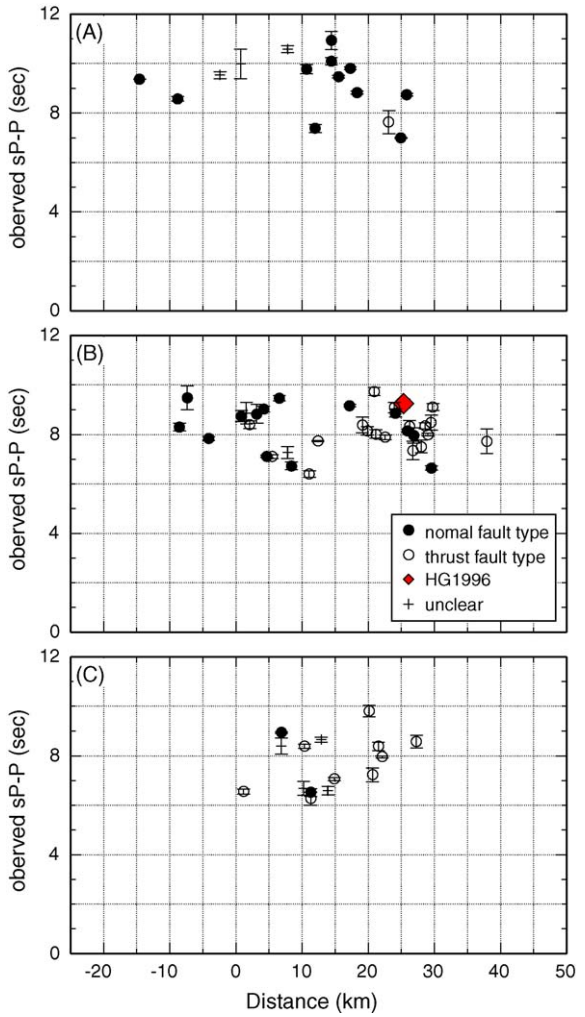

Fig. 6. Observed sP − P times for three areas (A–C) (see Fig. 2). Solid circles, open circles and diamond-shaped symbols indicate normal fault type and thrust fault type earthquakes, respectively. Large diamond-shaped symbol is for HG1996.

eral studies as discussed above. Fig. 7b also shows the P-wave velocity structure for a limited region (dotted frame of Fig. 7a) and the numbers within the parentheses denote the V_p/V_s ratios based on the results by Ludwig et al. (1970). We estimate theoretical travel-times using two-dimensional ray-tracing method, which is effective to examine the velocity structure from travel-times by try and error. We used ray-tracing programs "RAY02" and "TPRAY02" developed by Iwasaki (1988). As we adopt a two-dimensional velocity structure model, we limit observation stations with an azimuthal angle of 270–330° for each event.

The sP − P time mainly depends on the velocity structure around the epicenters. Thus, thick sedimentary layer and thin unconsolidated sedimentary layer in the Hyu-

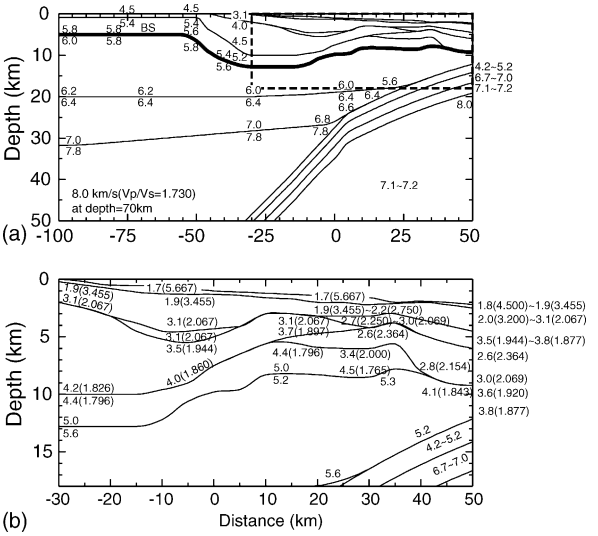

Fig. 7. (a) Cross-sectional view of the P-wave velocity structure model used in this study. (b) P-wave velocity structure for large scaled cross-sectional view of a's dotted frame corresponding to the area by Ichikawa (1997). The numbers within the parentheses denote the ratios of V_p/V_s based on the results by Ludwig et al. (1970). The point of 0 km corresponds to the peak position of the negative gravity anomaly for region B (see also Fig. 2). The V_p/V_s ratios above the line indicated by BS are based on the results by Ludwig et al. (1970) and those below are 1.73.

ganada region, locating around the peak position of negative free-air gravity anomaly (Fig. 2b), play an important role on the identification of sP phase. That is, three possibilities are expected for the reflection surface of observed sP phases, i.e. sP phase reflected at the ocean bottom, sP phase reflected at the bottom of unconsolidated layer and sP phase reflected at the bottom of sedimentary layer. These phases are referred to as sP1, sP2 and sP3 here, respectively. Fig. 8a–c show theoretical travel time differences for sP1 − P, sP2 − P and sP3 − P in regions A–C in Fig. 2, respectively. We, of course, checked that the theoretical sP − P time is insensitive to the epicentral distance for greater than 200 km as indicated by observations shown in Fig. 4.

The observed sP − P times are about 6–12 s (see Fig. 6), and the focal depths determined by sP − P times are also shown in Fig. 8, in which the epicenters were relocated using the focal depths determined by sP − P times. In order to confirm validity of focal depths using sP − P times, we used observed sP − P times for an event occurred on October 19, 1996. This event with $M_w = 6.7$, referred to as HG1996 here, is an interplate earthquake, and the recent observational studies (Uehira et al., 2001) indicate that the depth of plate boundary for its hypocenter is about 20 km. Also in the seismograms of the HG1996, the distinct later phase (X phase)

which has the same feature as sP phase is recognized 5–10 s after the P-wave onset. There is a possibility that the X phase is a multiple-shock phase because the source duration of the HG1996 is longer than the X − P time and is estimated to be 17 s (Yagi et al., 1999). The observed X − P time, however, depends on the epicentral distances shorter than 200 km. We therefore identified the X phase as sP phase. The observed sP − P time for this event is about 9.24 s on an average. The focal depth is also shown in Fig. 8. The focal depth distributions for regions A–C (see Fig. 2b) are separately depicted in these figures, and the region B corresponds to the central part of negative gravity anomaly. The observed sP phases cannot be explained by the reflection at the ocean bottom (sP1) because the focal depths are too shallow (Fig. 8a). It is, however, impossible to determine whether identified sP phases are reflected at the bottom of unconsolidated layer (sP2) or at the top of the basement (sP3). In the next section, we discuss geophysical implications for these results.

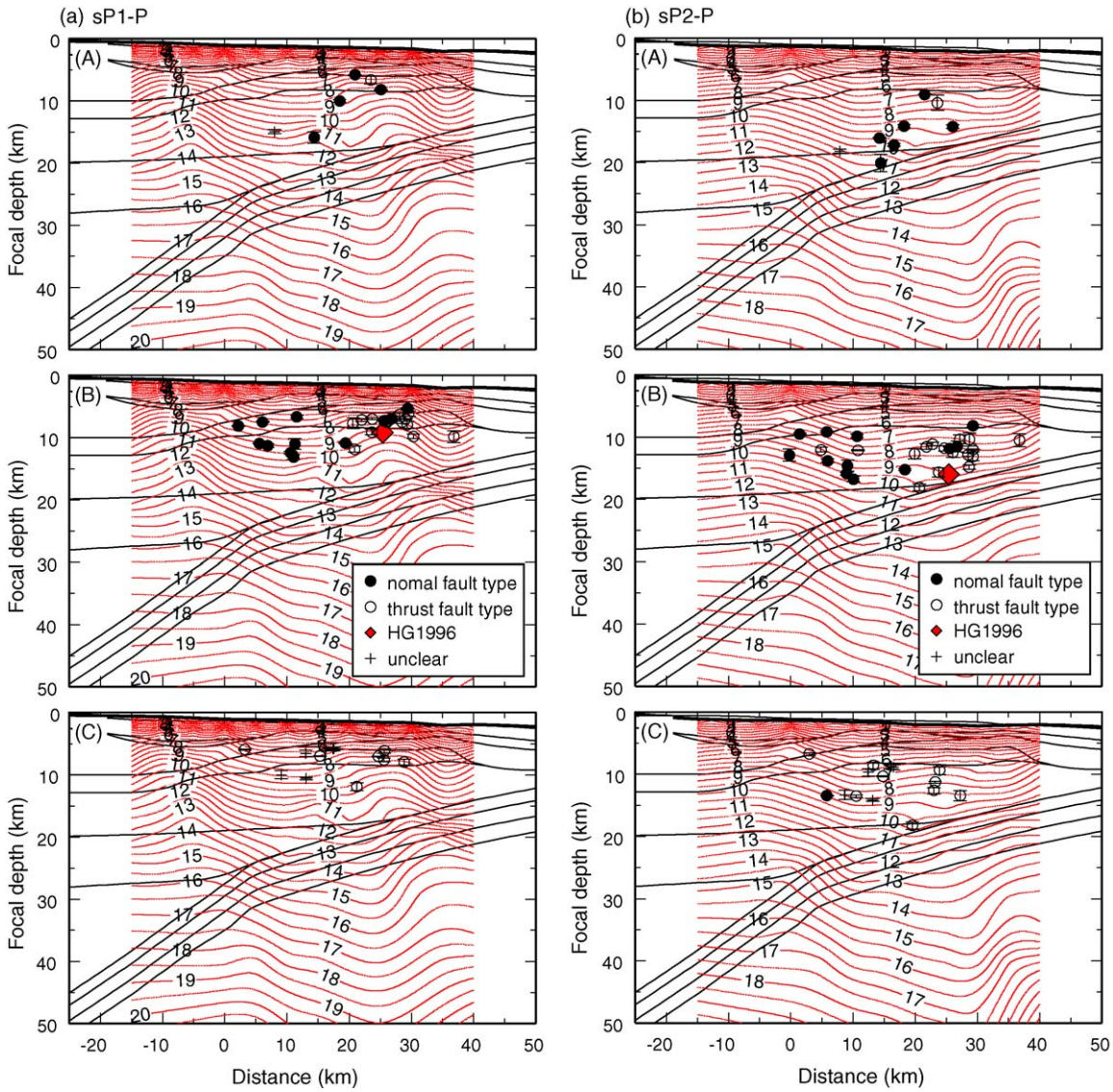

Fig. 8. Contour maps of theoretical sP − P times using ray-tracing method and focal depths using sP − P times for three areas (A–C). We examined three reflected positions and each reflection position is indicated by bold line. The reflection positions of sP phase are: (a) the ocean bottom, (b) the bottom of unconsolidated layers and (c) the top of basement. These phases are referred to as sP1, sP2 and sP3 here, respectively. Symbols are the same as those for Fig. 7.

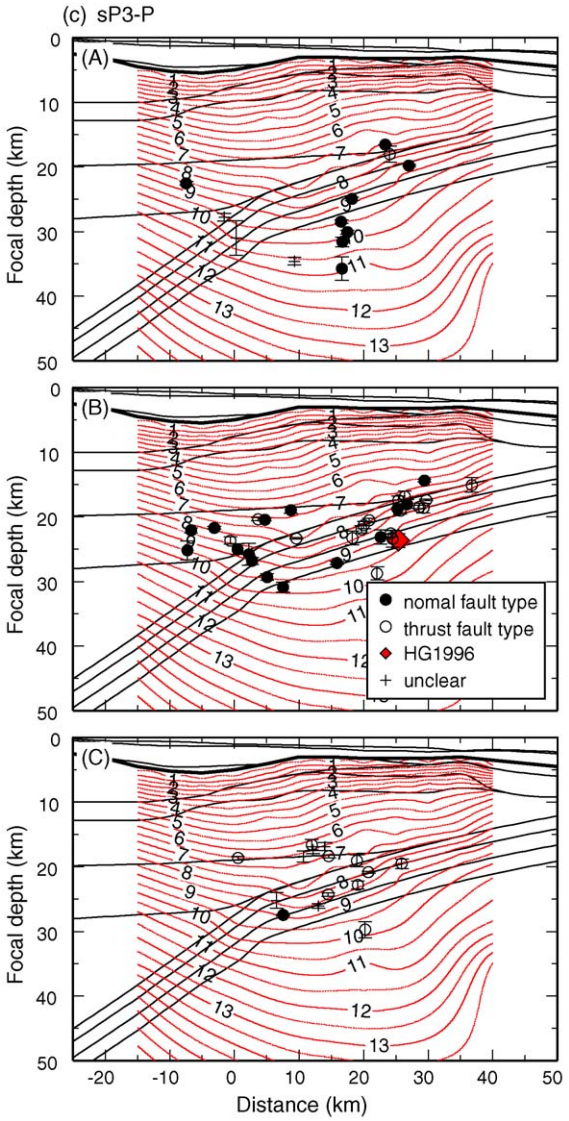

Fig. 8. (*Continued*).

5. Discussion and concluding remarks

The Miyazaki Plain is characterized by both significant negative gravity anomalies and aseismic crustal uplift in the Late Pleistocene. On the other hand, the feature for occurrences of great events around the Hyuganada region seems to be significantly different from that for off the Shikoku and Kii Peninsula (Ando, 1975; Kumagai, 1996). In order to understand the relationship for these observations, we examined the focal depth distributions using sP depth phases for events with $M \geq 3.5$. Based on the characters indicated by Umino et al. (1995), we could identify sP depth phases for 90% events examined here. It is, however, difficult to determine the reflection surface of sP phase, i.e. the ocean bottom (sP1) or the bottom of the unconsolidated layer (sP2) or the top of the basement (sP3), because the adopted velocity structure for the Hyuganada region, particularly for S-wave velocity, has not been determined accurately. While the adopted P-wave velocity model may be applicable to the structure for region B (see Fig. 2), it may be difficult to apply the adopted model to those for regions A and C.

As shown in Fig. 8, the focal depth for event of HG1996 does not coincide with the plate boundary. Reading errors for arrival times of sP phases insignificantly affect the focal depths as shown in Figs. 8 and 9. However, there is no doubt that uncertainties of adopted velocity structure significantly affect the focal depths. Here we tentatively change the ratios of V_p/V_s and modify the velocity model, in which the focal depths of HG1996 and thrust type events coincide with the plate boundary. If we assume that the sP depth phases are reflected at the ocean bottom, then the focal depths are too shallow (Fig. 8a). Here we therefore assume that the observed depth phases reflected at the bottom of unconsolidated layer or at the top of the basement. The focal depth distributions for modified models are shown in Fig. 9a and b. While the conversion efficiency (e.g. Aki and Richards, 1980) for sP3 is about one to five times larger than that for sP2, it is difficult to definitely determine the reflection surface of sP phase, i.e. sP2 or sP3. That is, the conversion efficiency depends on both the reflection angle and reflection surface. Fig. 9a shows the focal depth distribution determined by sP2 − P, i.e. reflected at the bottom of unconsolidated layer. In this case, we adopted the ratios of $V_p/V_s = 1.73$ for all regions. Fig. 9b depicts the focal depth distribution for sP3 − P, i.e. reflected at the top of the basement. The velocity model for sP3 − P is reconstructed by assuming that V_p/V_s ratios are 1.15 times for those by Ludwig et al. (1970).

We can find some interesting features in the distributions of seismicity shown in Fig. 9 (see also Fig. 8). That is, most events in the northern area (region A) are normal fault type and those for the southern area (region C) are thrust fault type. While the focal depths depend on an adopted velocity model, the difference between regions A and C is probably insensitive to velocity model as inferred from observed sP − P (Fig. 6). In contrast, each type event generally occurs in clusters for region B around the central part of negative gravity anomaly, and there is a seismicity gap between each cluster. In addition, focal depth distributions for region B are significantly different in the western and eastern parts. That is, a lot of tensile events occur in the western part around the minimum peak for gravity anomalies (region I in

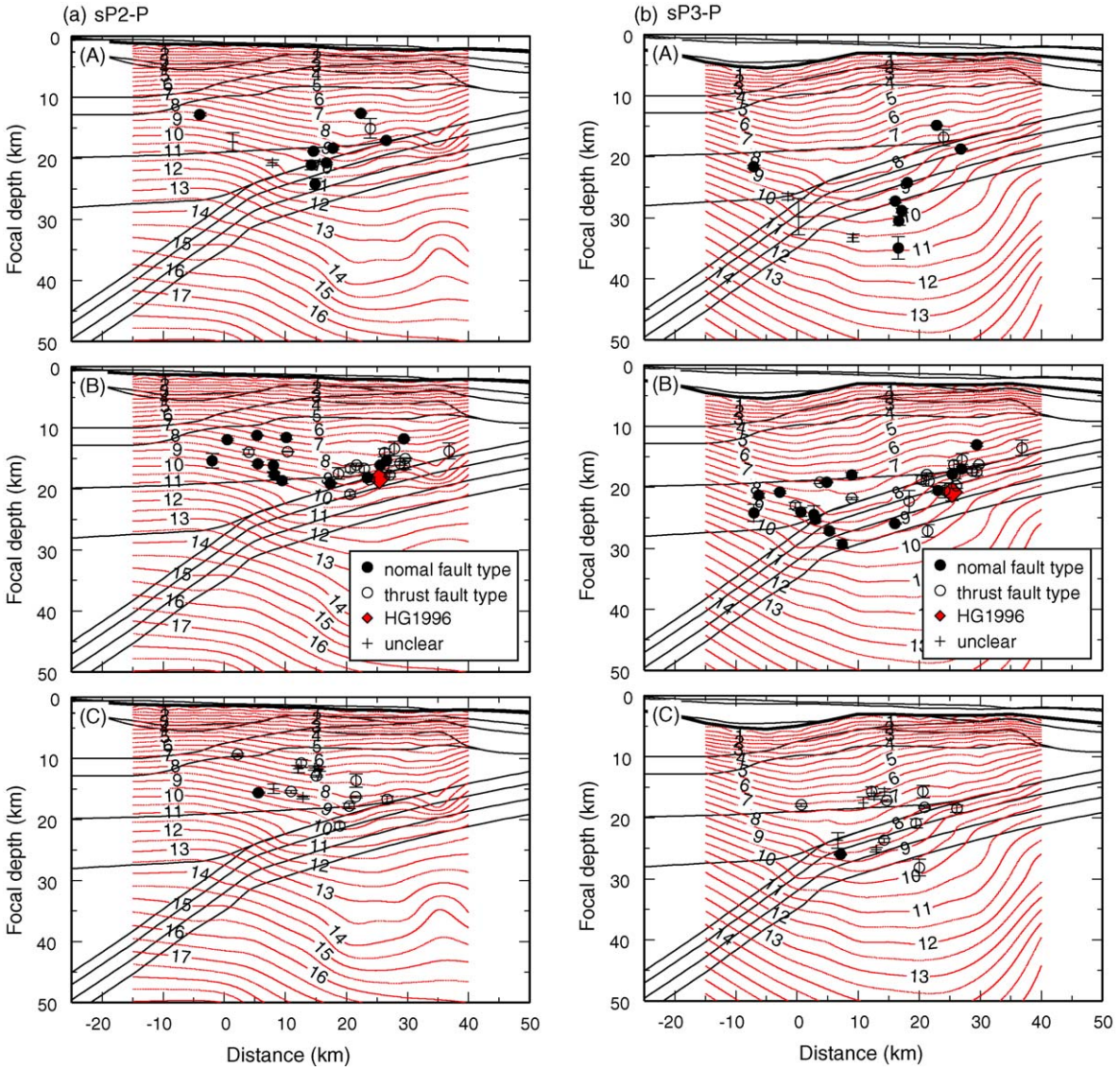

Fig. 9. As in Fig. 8 for the cases of sP2 and sP3 phases. We changed the ratios of V_p/V_s and modified the velocity model in which the focal depth of HG1996 and low-angle reverse fault type earthquakes coincide with the plate boundary. (a) For sP2 − P times with $V_p/V_s = 1.73$ for all regions. (b) For sP3 − P times with 1.15 times V_p/V_s for those by Ludwig et al. (1970).

Fig. 1b and c) and thrust type events occur in the eastern part as usual case (region II in Fig. 1b and c). In the case for sP2 − P (Fig. 9a), the compressional events occur near the plate boundary and tensile events occur above 20 km depth. The focal depth distribution of tensile events for sP2 − P approximately corresponds to the boundary between the upper crust and the lower crust. In the case of sP3 − P (Fig. 9b), the tensile events occur in the lower crust and around the plate boundary. Both results for sP2 − P or sP3 − P indicate a tensional state for the area around the peak position of negative gravity anomalies.

Fig. 10a and b show the projections of the *P* and *T*-axes of the focal mechanisms in region B for cases of sP2 − P (reflection at the bottom of unconsolidated layer) and sP3 − P (reflection at the top of the basement), respectively. We redetermined the MT solutions by using relocated focal depths and confirmed that NIED's MT solutions do not change even if the differences between the original and relocated focal depths reach 30 km. However, we removed the events with the difference of greater than 30 km, and those events are denoted by asterisk in Table 1. We first discuss the stress states for events of the western part. In the case of sP2 − P, the

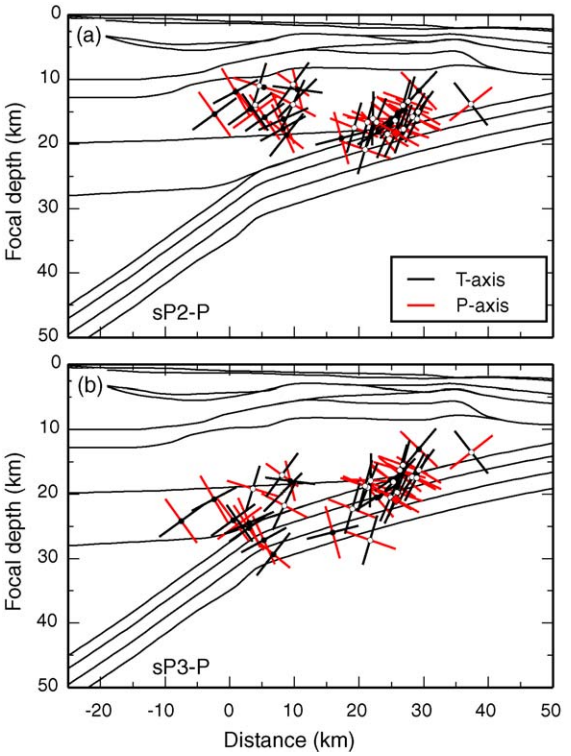

Fig. 10. Cross-sectional views of focal depths using sP − P times and the projections of *P* and *T*-axes in region B for (a) sP phases reflected at the bottom of unconsolidated layer (sP2) and (b) sP phases reflected at the top of basement (sP3).

T-axes for events occurred in the lower part of the upper crust are generally parallel to the subducting slab and those *P*-axes are normal to the slab. This result seems to be consistent with the underplating load model proposed by Nakada et al. (2002). If the underplating load, corresponding to the negative gravity anomalies, exists beneath the Moho, the stress states of the upper and lower crust may be expected to be tensile and compressional, respectively. On the other hand, the results for sP3 − P indicate that the *T*-axes for events occurred in the lower crust and around the plate boundary are parallel to the subducting slab. In this case, tensile events may occur in the source area for the negative gravity anomalies. The events for the plate boundary may be associated with the bending of subducting slab probably caused by the buoyant body.

The western part for the tensile events is denoted by region I in Fig. 1b and c. On the other hand, the *P*-axes for events of the eastern part indicate that these events are thrust type earthquakes and occur around the plate boundary. The eastern part corresponds to the western edge of the Hyuga Basin, denoted by II in Fig. 1b and c. This region may correspond to the asperity area of 1968 Hyuganada earthquake (Yagi and Kikuchi, 2003) and also the area with the relationship between the asperities and prominent free-air gravity anomaly indicated by Wells et al. (2003). The significant gravity low of the western part is, however, distinguished from the gravity low corresponding to that indicated by Wells et al. (2003). In fact, the gradient for region II in Fig. 1b seems to be different from those for I and III, and the relationship using 1968 Hyuganada earthquake by Wells et al. (2003) may not applicable to the events for the central part of Hyuga Basin. We depict a hypothetical gravity anomaly profile by dashed line in Fig. 1b, inferred from the observed gradients for regions I and III. We speculate that the relative gravity low with ∼−30 mgal, derived from the differences using these two profiles, may correspond to the gravity low indicated by Wells et al. (2003). The magnitude obtained here, i.e. ∼−30 mgal, is similar to that for the gravity lows discussed by Wells et al. (2003). So, observed negative gravity anomalies for this region may be caused by two different sources.

Thus, the seismicity patterns are very different in these regions and the events with $M_w \geq 3.5$, for a period from January 1997 to September 2001, have not been observed in the boundary region. While we cannot determine the focal mechanisms and focal depths for events with $M_w < 3.5$, it is not unreasonable to assume that a number of tensile events have occurred in the crust around the minimum gravity anomalies. It may be possible to point out possible causes for the source of negative gravity anomalies around the Hyuganada region, i.e. subduction of Kyushu Palau ridge (Nagaoka et al., 1991), an accumulation of sediments associated with subduction (Walcott, 1987; Reyners and McGinty, 1999), serpentinized wedge mantle (Kamiya and Kobayashi, 2000) and accumulated lower crust (Nakada and Takeda, 1995). Although we have no answer for this problem, the present study indicates a clear correlation between the seismicity and the gravity anomaly. If we adopt the results for sP2 − P shown in Fig. 10a, then it may be possible to make a scenario that the steady upward movement associated with the buoyant body causes the tensile events of the crust and a few relatively small asperities of the M_w 7 class earthquakes for off the Miyazaki Plain (e.g. Kawasaki, 2004). On the other hand, if we adopt the result for sP3 − P shown in Fig. 10b, it may be possible to speculate that the buoyant body bends the subducting plate and the tensile bending stress of the subducting slab is a cause of normal fault type earthquakes with *T*-axes parallel to the subducting slab. In order to examine these points in more detail, however, we require a high-resolution tomography for the Hyuganada region.

Acknowledgments

We thank K. Uehira for the use of SEVO data and T. Iwasaki for the use of ray-tracing programs 'RAY02' and 'TPRAY02'. We also thank NIED and JMA for the use of seismic information, and K. Uehira, A. Kubo and S. Matsumoto for their valuable comments and discussion. This work was partly supported by Japanese Ministry of Education, Science and Culture to M.N. (Grand-in Aid for Science Research No. 14540396 and No. 17340132). A software packages, the Generic Mapping Tools (GMT), were used to plot figures.

References

Aki, K., Richards, P.G., 1980. Quantitative Seismology. W.H. Freeman, New York.

Ando, M., 1975. Source mechanisms and tectonic significance of historical earthquakes along the Nankai Trough Japan. Tectonophysics 27, 119–140.

Dziewonski, A.M., Chou, T.A., Woodhouse, J.H., 1981. Determination of earthquake source parameters from waveform data for studies of global and regional seismicity. J. Geophys. Res. 86, 2825–2852.

Fukumitsu, S., Miyamachi, H., Kakuta, T., Goto, K., Umakoshi, K., Shimizu, H., 1997. Pn velocity in Kyushu deduced from travel time analysis of local earthquakes. J. Seism. Soc. Jpn. 50, 353–356 (in Japanese).

Fukuyama, E., Ishida, M., Dreger, D.S., Kawai, H., 1998. Automated seismic moment tensor determination by using on-line broadband seismic waveforms. J. Seism. Soc. Jpn. 51, 149–156 (in Japanese and English abstract).

Geological Survey of Japan, 2000. Gravity CD-ROM of Japan. Geological Survey of Japan, Tsukuba, Japan.

Hirose, H., Hirahara, K., Kimata, F., Fujii, N., Miyazaki, S., 1999. A slow thrust slip event following the two 1996 Hyuganada earthquakes beneath the Bungo Channel, southwest Japan. Geophys. Res. Lett. 26, 3237–3240.

Hyndman, R.D., Wang, K., Yamano, M., 1995. Thermal constraints on the seismogenic portion of the southwestern Japan subduction thrust. J. Geophys. Res. 100, 15373–15392.

Ichikawa, G., 1997. Ocean Bottom Seismographic Experiment to Study Crustal Structure in Hyuga-nada. M.Sc. Thesis, University of Hokkaido (in Japanese).

Iwasaki, T., 1988. Ray-tracing program for study of velocity structure by ocean bottom seismographic profiling. J. Seism. Soc. Jpn. 41, 263–266 (in Japanese).

Iwasaki, T., Kato, W., Moriya, T., Hasemi, A., Umino, N., Okada, T., Miyashita, K., Mizogami, T., Takeda, T., Sekine, S., Matsushima, T., Tashiro, K., Miyamachi, H., 2001. Extensional structure in northern Honshu arc as inferred from seismic refraction/wide-angle reflection profiling. Geophys. Res. Lett. 28, 2329–2332.

Kamata, H., Kodama, K., 1993. The Hohi volcanic zone as a volcanotectonic depression and its formation tectonics-three tectonic events caused by subduction of the Philippine Sea Plate under the junction of the Southwest Japan Arc and the Ryukyu Arc. Mem. Geol. Soc. Jpn. 41, 129–148 (in Japanese with English abstract).

Kamiya, S., Kobayashi, Y., 2000. Seismological evidence for the existence of serpentinized wedge mantle. Geophys. Res. Lett. 27, 819–822.

Kanamori, H., 1977. The energy release in great earthquakes. J. Geophys. Res. 82, 2981–2987.

Kato, T., El-Fiky, G.S., Oware, E.N., Miyazaki, S., 1998. Crustal strains in the Japanese islands as deduced from dense GPS array. Geophys. Res. Lett. 25, 3445–3448.

Kawasaki, I., 2004. Silent earthquakes occurring in a stable-unstable transition zone and implications for earthquake prediction. Earth Planets Space 56, 813–821.

Kennett, B.L.N., Engdahl, E.R., 1991. Traveltimes for global earthquake reference location and phase identification. Geophys. J. Int. 105, 429–465.

Kobayashi, K., Nakada, M., 1978. Magnetic anomalies and tectonic evolution of the Shikoku inter-arc basin. J. Phys. Earth 26, S391–S402.

Kono, Y., Furuse, N., 1989. Gravity Anomaly Map in and Around the Japanese Islands. University of Tokyo Press, Tokyo, Japan.

Kumagai, H., 1996. Time sequence and the recurrence models for large earthquakes along the Nankai Trough revisited. Geophys. Res. Lett. 23, 1139–1142.

Lay, T., Kanamori, H., 1981. An asperity model of great earthquake sequences. In: Simpson, D., Richards, P. (Eds.), Earthquake Prediction: An International Review, Maurice Ewing Ser., vol. 4. AGU, Washington, DC, pp. 579–592.

Ludwig, W.J., Nafe, J.E., Drake, C.L., 1970. Seismic refraction. In: Maxwell, A.E. (Ed.), The Sea, vol. 4, Ideas and Observations on Progress in the Study of the Seas. Wiley-Interscience, New York.

Mogi, K., 1969. Relationship between the occurrence of great earthquakes and tectonic structures. Bull. Earthquake Res. Inst. Univ. Tokyo 47, 429–451.

Nagaoka, S., 1986. The landform evolution of Late Pleistocene in the Miyazaki Plain, South Kyushu. Jpn. Quat. Res. (Japan) 25, 139–163 (in Japanese with English abstract).

Nagaoka, S., Maemoku, H., Matsushima, Y., 1991. Evolution of Holocene coastal landforms in the Miyazaki Plain, southern Japan. Quat. Res. (Japan) 30, 59–78 (in Japanese with English abstract).

Nakada, M., Takeda, Y., 1995. Roles of mantle diapir and ductile lower crust on island-arc tectonics. Tectonophysics 246, 147–161.

Nakada, M., Tahara, M., Shimizu, H., Nagaoka, S., Uehira, K., Suzuki, S., 2002. Late Pleistocene crustal uplift and gravity anomaly in the eastern part of Kyushu, Japan, and its geophysical implications. Tectonophysics 351, 263–283.

Nakamura, M., 2002. Estimate of Moho discontinuity by using converted wave in seismograms of intermediate earthquakes beneath the Kyushu district, Japan. M.Sc. Thesis, Kyushu University (in Japanese).

Nakamura, M., Watanabe, H., Konomi, T., Kimura, S., Miura, K., 1997. Characteristic activities of subcrustal earthquakes along the outer zone of southwestern Japan. Ann. Disast. Prev. Res. Inst., Kyoto Univ. 40, 1–20 (in Japanese).

Obara, K., 2002. Nonvolcanic deep tremor associated with subduction in southwest Japan. Science 296, 1679–1681.

Ono, K., Ito, K., Hasegawa, I., Ichikawa, K., Iizuka, S., Kakuta, T., Suzuki, H., 1978. Explosion seismic studies in south Kyushu especially around the Sakurajima Volcano. J. Phys. Earth 26, S309–S319.

Ota, Y., Omura, A., 1991. Late Quaternary shorelines in the Japanese Islands. Quat. Res. (Japan) 30, 175–186.

Reyners, M., McGinty, P., 1999. Shallow subduction tectonics in the Raukumara Peninsula, New Zealand, as illuminated by earthquake focal mechanisms. J. Geophys. Res. 104, 3025–3034.

Scott, D.R., Kanamori, H., 1985. On the consistency of moment tensor source mechanisms with first motion data. Phys. Earth Planet. Int. 86, 223–241.

Seno, T., Stein, S., Gripp, A.E., 1993. A model for the motion of the Philippine Sea Plate consistent with NUVEL-1 and geological data. J. Geophys. Res. 89, 17941–17948.

Stein, S., Wiens, D.A., 1986. Depth determination for shallow teleseismic earthquakes Methods and results. Rev. Geophys. 24, 806–832.

Tashiro, K., Suzuki, S., Matsushima, T., Miyamachi, H., Iwasaki, T., Yoshii, T., Takeda, T., Piao, C., Sakai, S., Iidaka, T., Kubo, A., Moriya, T., Ando, M., 1999. Upper crustal structure in the eastern part of Kyushu, Japan, inferred from seismic refraction experiments. Sci. Rep. Dept. Earth Planet. Sci., Kyushu Univ. 20, 111–123 (in Japanese with English abstract).

Uehira, K., Shimizu, H., Matsuwo, N., Goto, K., 2001. The detailed structure of the deep seismic zone and focal mechanism solutions in and around the Kyushu district Japan. Earth Monthly 23, 669–673 (in Japanese).

Umino, N., Hasegawa, A., Matsuzawa, T., 1995. sP depth phase at small epicentral distances and estimated subducting plate boundary. Geophys. J. Int. 120, 356–366.

Utsu, T., 1974. Space-time pattern of large earthquakes occurring off the Pacific coast of the Japanese islands. J. Phys. Earth 22, 325–342.

Walcott, I.R., 1987. Geodetic strain and the deformational history of the North Island of New Zealand during the late Cenozoic. Philos. Trans. R. Soc. Lond. Ser. A 321, 163–181.

Wang, K., Suyehiro, K., 1999. How does plate coupling affect crustal stresses in Northeast and Southwest Japan? Geophys. Res. Lett. 26, 2307–2310.

Wells, R.E., Blakely, R.J., Sugiyama, Y., Scholl, D.W., Dinterman, D.A., 2003. Basin-centered asperities in great subduction zone earthquakes: a link between slip, subduction and subduction erosion. J. Geophys. Res. 108 (B10), 2507, doi:10.1029/2002JB002072.

Yagi, Y., Kikuchi, M., Yoshida, S., Sagiya, T., 1999. Comparison of the coseismic rupture with the aftershock distribution in the Hyuganada earthquakes of 1996. Geophys. Res. Lett. 26, 3161–3164.

Yagi, Y., Kikuchi, M., Sagiya, T., 2001. Co-seismic slip, post-seismic slip, and aftershocks associated with two large earthquakes in 1996 in Hyuga-nada, Japan. Earth Planets Space 53, 793–803.

Yagi, Y., Kikuchi, M., 2003. Partitioning between seismogenic and aseismic slip as highlighted from slow slip events in Hyuganada. Jpn. Geophys. Res. Lett. 30 (2), 1087, doi:10.1029/2002GL015664.

Yoshii, T., 1979. A detailed cross-section of the deep seismic zone beneath northeastern Honshu Japan. Tectonophysics 55, 349–360.